Monthly Notices of the ROYAL ASTRONOMICAL SOCIETY

MNRAS **527,** 10726–10736 (2024) https://doi.org/10.1093/mnras/stad3909
Advance Access publication 2023 December 19

ExoMol line lists – LII. Line lists for the methylidyne cation (CH^+)

Oliver Pearce, Sergei N. Yurchenko and Jonathan Tennyson ★
Department of Physics and Astronomy, University College London, Gower Street, WC1E 6BT London, UK

Accepted 2023 December 18. Received 2023 December 7; in original form 2023 July 12

ABSTRACT

Comprehensive and accurate rovibronic line lists for the $X\,^1\Sigma^+$ and $A\,^1\Pi$ states of $^{12}C^1H^+$ and $^{13}C^1H^+$ which should be applicable up to temperatures of 5000 K are presented. Available empirical potential energy curves and high-level *ab initio* dipole and transition dipole moment curves are used with the program LEVEL to compute rovibronic energy levels and Einstein *A* coefficients. Λ-doubling is incorporated into the energy levels and *A*-coefficients involving the $A\,^1\Pi$ state using an empirical method. For $^{12}C^1H^+$, line positions are improved by using both laboratory and astronomical observational spectra as input to the MARVEL (Measured Active Rotational-Vibrational Energy Levels) procedure. The $^{12}C^1H^+$ line list contains 1505 states and 34 194 transitions over the frequency range of 0–33 010 cm^{-1} ($\lambda > 300$ nm). Comparisons with observed astronomical and laboratory spectra give very good agreement. The PYT CH^+ line lists and partition functions are available from the ExoMol database at www.exomol.com.

Key words: molecular data – opacity – exoplanets – planets and satellites: atmospheres – ISM: molecules.

1 INTRODUCTION

The methylidyne cation, CH^+, was one of the first molecules, and the first molecular ion, to be detected in space (Dunham 1937). CH^+ has since been found to be ubiquitous in interstellar space (Godard et al. 2023) where it has been observed both in absorption and emission in various cool environments (Dunham 1937; Crawford 1989; Gredel, Van Dishoeck & Black 1993; Cernicharo et al. 1997; Naylor et al. 2010; York et al. 2013; Krelowski, Galazutdinov & Bondar 2020; Neufeld et al. 2021) which include protostellar discs (Thi et al. 2011), diffuse clouds (Crane, Lambert & Sheffer 1995), and lines of sight towards star-forming regions (Falgarone et al. 2010), with even routine detection from extragalactic sources (Rangwala et al. 2011; Ritchey et al. 2015; Falgarone et al. 2017; Muller et al. 2017). In addition, strong CH^+ $A\,^1\Pi - X\,^1\Sigma^+$ emission spectra have been observed in the red rectangle (post-asymptotic giant branch star HD 44179), see Hobbs et al. (2004), and references therein. The ratio of $^{13}CH^+$ to $^{12}CH^+$ absorption spectra have been extensively studied to monitor the interstellar $^{13}C/^{12}C$ abundance ratios, see Stahl, Casassus & Wilson (2008) and Ritchey et al. (2015), and references therein.

Astrophysical interest in CH^+ has sparked many investigations; these include using its unique properties, which allow tracing of significant energy releases and interstellar turbulence (Vidal-García et al. 2022), and its importance in astrochemistry, particularly for helping to understand diffuse interstellar clouds. CH^+ is thought to be a building block for the formation of organic molecules in interstellar space, principally through its role as an intermediary in reactions producing larger hydrocarbons (Barinovs & van Hemert 2004; Domenech et al. 2018), and molecules including C_2, CN, CO, and CH (Hakalla et al. 2007). Furthermore, owing to its efficient destruction mechanisms (Gredel et al. 1993) and inherently reactive nature with species prevalent in its environment (most notably H and H_2), it came as a great surprise when the abundance of the molecule was observed to exceed predictions by several orders of magnitude (Dalgarno 1976). This has stimulated significant investigation into the formation, destruction and abundance of CH^+ over many years (Gredel et al. 1993; Gredel 1997; Wesson et al. 2010; Falgarone et al. 2010; Valdivia et al. 2017). While the primary formation mechanism and observed abundance of CH^+ remain in question, some recent studies have begun to provide explanations that reduce the large discrepancy between calculation and observation (Faure et al. 2017; Godard et al. 2023).

Interest in CH^+ has also motivated a number of laboratory studies. Its rovibronic spectrum (involving vibrationally and rotationally resolved transitions between electronic states) has been widely studied (Douglas & Herzberg 1942; Douglas & Morton 1960; Botterud, Lofthus & Veseth 1973; Cosby, Helm & Moseley 1980; Grieman et al. 1981; Carrington & Ramsay 1982; Helm et al. 1982a; Carrington & Softley 1986; Sarre, Walmsley & Whitham 1986; Hechtfischer et al. 2002; Dubois & Lefebvre 2004; Hakalla et al. 2006; Hechtfischer et al. 2007; Mueller 2010; Yu et al. 2018), most notably the $A\,^1\Pi - X\,^1\Sigma^+$ (A-X) system which covers transitions between the two lowest energy singlet states. Landmark studies include the work by Carrington & Ramsay (1982), the first high-resolution study (uncertainty ≤0.01 cm^{-1}) which also assigned many transitions involving low vibrational levels ($v'' = 0$–3), and more recently that of Hakalla et al. (2006) who comprehensively characterized low vibrational bands. The pure rotational spectrum of CH^+, first detected in space through emission lines from a planetary nebula (Cernicharo et al. 1997), has received much less coverage with only a few low-energy lines being observed so far. The first laboratory detection of a pure rotational line ($J = 1 - 0$, Pearson &

★ E-mail: j.tennyson@ucl.ac.uk

Table 1. Summary of spectroscopic laboratory and astronomically observed papers used in our ^{12}CH MARVEL study.

Reference	Freq. range (cm^{-1})	Detected transitions[a]	A/V[b]	Uncert[c] (cm^{-1})
21NeGoChFa (Neufeld et al. 2021)	2422.62–2942.57	(1,0): $J'' \leq 10$	16/16	3×10^{-2}
18DoJuScAs (Domenech et al. 2018)	27.85719	(0,0): R(0)	5/5	2×10^{-5}
	2711.81–2817.23	(1,0): $J'' \leq 3$		
15YuDrPeAm (Amano et al. 2015)	55.68–83.44	(0,0): R(1), R(2)	2/2	3×10^{-6}
10Amano (Amano 2010b)	27.85719	(0,0): R(0)	1/1	7×10^{-7}
06PeDr (Pearson & Drouin 2006)	27.85523	(0,0): R(0)	1/0	3×10^{-6}
06HaKeSzZa (Hakalla et al. 2006)	20401.56–23967.41	(0,0),(0,1),(2,1): $J'' \leq 17$	124/124	1×10^{-2}
02HeWiLaLi (Hechtfischer et al. 2002)	31747.0–33000.0	(11, 0), (12, 0), (13, 0), (14, 0): $J'' \leq 9$	35/35	1
97CeLiGoCo (Cernicharo et al. 1997)	55.68–165.92	(0, 0): $J'' = 1 - 5$	6/6	5×10^{-2}
89SaWhGr (Sarre, Whitham & Graff 1989)	16750–18613	(0, 1), (1, 1), (2, 1): $J'' = 32–35$	6/6	1
86SaWaWh (Sarre et al. 1986)	16125.31– 18613.07	(0,0),(0,1),(1,1),(1,2),(2,1), (2, 2), (3, 2), (3, 3), (4, 3), (5, 3), (5, 4), (7, 4), (7, 5): $J'' = 18 - 35$	29/29	5×10^{-3}
82CaRa (Carrington & Ramsay 1982)	17111.40–25281.30	(0,0),(0,1),(1,0),(1,1),(1,2), (1, 3), (2, 1), (3, 1): $J'' \leq 14$	231/231	1×10^{-2}
82HeCoGrMo (Helm et al. 1982a)	15460–28484	Many $v' \leq 10$ vibrational bands: $J'' = 11–36$	51/51	1
81GrBrOkWi (Grieman et al. 1981)	22540.0–23615.1	(0, 0): $J'' = 6–21$	36/36	1×10^{-1}
80CoHeMo (Cosby et al. 1980)	27494–28523	Transitions unassigned	N/A	1×10^{-2}
60DoMo (Douglas & Morton 1960)	20524.30–26266.21	(0, 1), (1, 1), (2, 1), (3, 1), (4, 1): $J'' \leq 15$	130/129	5×10^{-2}
42DoHe (Douglas & Herzberg 1942)	20636.8–26704.1	(0, 0), (0, 1), (1, 0), (2, 0): $J'' \leq 11$	94/94	2×10^{-1}

Notes. [a]Bracketed values indicate the vibrational bands involved in transition, (v', v'').
[b]'A/V': number of actual lines in source/number of lines validated by MARVEL.
[c]Uncert: average uncertainty as quoted (if available), or the modified uncertainty for the MARVEL algorithm.

Drouin 2006) was later proven to be inaccurate by 0.0019 cm^{-1} and its frequency was superseded by later studies (Amano 2010b; Domenech et al. 2018). The rovibrational spectrum has proven more elusive still, the first and only high-resolution laboratory study was made by Domenech et al. (2018), and the corresponding astronomical detection only from one source, NGC 7027 (Neufeld et al. 2021). The minor isotopologues, most notably $^{13}CH^+$ and $^{12}CD^+$, have also received significant spectroscopic investigation (Antić-Jovanovic et al. 1983; Bembenek, Cisak & Kepa 1987; Bembenek 1997; Amano 2010b; Dubois & Lefebvre 2004; Hechtfischer et al. 2007; Amano et al. 2015; Yu et al. 2018; Domenech et al. 2018). A summary of the spectroscopic laboratory and astronomically observed literature used in this study that covers the relevant electronic states, $X\,^1\Sigma^+$ and $A\,^1\Pi$, is given in Table 1. Some papers provide spectroscopic analysis but do not present new line data (Hakalla et al. 2007; Mueller 2010; Amano 2010a; Amano 2015; Yu et al. 2018).

Theoretical investigations have aimed to characterize the potential energy curves (PECs) and dipole/transition dipole moments (DMs/TDMs) of CH^+. PECs, unique to each electronic state, describe the potential energy of an electron as a function of nuclear distance, while DMs/TDMs describe the strength of interaction between two different states during a transition between them. Many *ab initio* electronic structure studies have focused on CH^+ since it contains just six electrons; these provide PECs for low-lying electronic states, notably $X\,^1\Sigma^+$, $A\,^1\Pi$, and $a\,^3\Pi$ (Sauer & Spirko 2013; Gao, Wu & Wan 2017; Changala, Neufeld & Godard 2021), with some also characterizing higher energy states (Saxon, Kirby & Liu 1980; Kanzler, Sun & Freed 1991; Kowalski & Piecuch 2001; Barinovs & van Hemert 2004; Biglari, Shayesteh & Maghari 2014; Babb & McLaughlin 2017; Mbiba Touedebe, Nkem & Owono Owono 2023). Here, we use the PECs due to Cho & Le Roy (2016) who used a fully empirical ('direct potential fit') approach that utilizes experimental data to fit the PECs of the $X\,^1\Sigma^+$ and $A\,^1\Pi$ states which, if sufficient experimental data is available, is a more accurate method than *ab initio* studies. The PECs of the three lowest electronic states of CH^+ can be seen in Fig. 1 (Gao et al. 2017). Several studies have characterized DMs/TDMs (Saxon et al. 1980; Kanzler et al. 1991; Sauer & Spirko 2013; Gao et al. 2017; Babb & McLaughlin 2017;Changala et al. 2021) with notable investigations covering a vast number of singlet, triplet, and quintet states using large basis sets and extending to large internuclear separations (Biglari et al. 2014; Chakrabarti et al. 2017; Mbiba Touedebe et al.

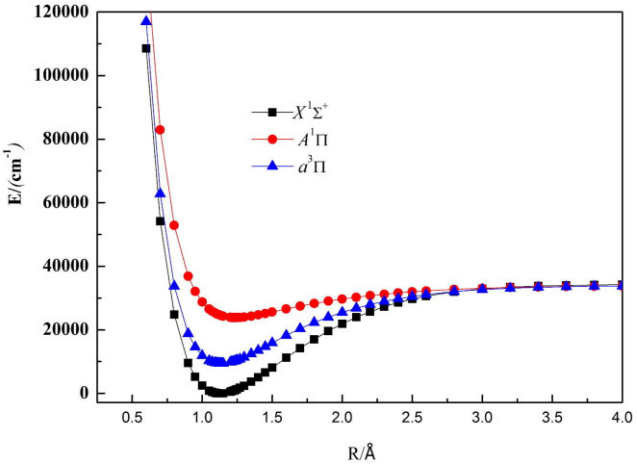

Figure 1. PECs for the low-lying electronic states below the first dissociation limit, $X\,^1\Sigma^+$, $A\,^1\Pi$, and $a\,^3\Pi$. Figure from Gao et al. (2017) Reprinted from Computational and Theoretical Chemistry, vol. 1117, Yufeng Gao, Tiantian Wu and Mingjie Wan, Ab initio electronic structure and transition properties of CH^+ isotope series including spin-orbit coupling, 276-284, Copyright (2017), with permission from Elsevier .

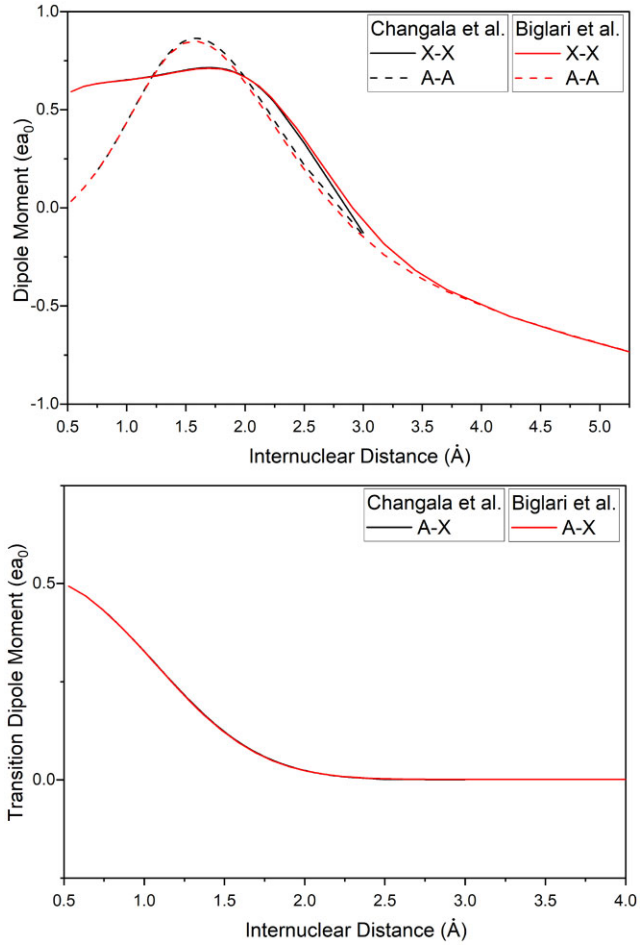

Figure 2. Comparison of DMs, in au, for the $X\,^1\Sigma^+$ and $A\,^1\Pi$ states (top) and TDMs for $A\,^1\Pi$ - $X\,^1\Sigma^+$ (bottom) from Biglari et al. (2014) and Changala et al. (2021).

2023). The curves were compared (where data were available) and were seen to agree well, particularly those of A-X. A comparison of the X-X and A-A DMs, and A-X TDMs from Biglari et al. (2014) and Changala et al. (2021) is shown in Fig. 2.

The ExoMol project aims to provide comprehensive spectroscopic data for transitions within molecules relevant to exoplanetary atmospheres, cool stars, and brown dwarfs (Tennyson & Yurchenko 2012). Since its inception, the project has created line lists for many diatomic molecules, ions, and larger polyatomic species, that comprehensively characterize the spectroscopic properties of the molecule and allows a model/profile to be built up. In this study, we calculate a comprehensive and accurate line list for the $X\,^1\Sigma^+$ and $A\,^1\Pi$ states of $^{12}C^1H^+$ and $^{13}C^1H^+$ as part of the ExoMol project.

2 METHODS

To calculate the line list of CH^+, quantum mechanical nuclear-motion calculations were performed using the program LEVEL (Le Roy 2017) which generated the desired energy levels and transition data. To verify and improve on the calculated data, existing experimental and observational spectroscopic data for CH^+ were gathered for use with the program MARVEL (Measured Active Rotational-Vibrational Energy Levels; Furtenbacher, Császár & Tennyson 2007). The MARVEL (Furtenbacher et al. 2007) algorithm inverts transition data to give highly accurate energy levels along with determined uncertainties.

2.1 MARVEL energy levels

767 $^{12}CH^+$ lines were collected from existing observational studies as summarized in Table 1. While most of the sources are from high-resolution laboratory studies, 97CeLiGoCo (Cernicharo et al. 1997) and 21NeGoChFa (Neufeld et al. 2021) are actually astronomical observations. Table 1 shows that there are rather few observed transitions within the $X\,^1\Sigma^+$ ground state of $^{12}CH^+$, hence the need to include astronomically observed lines which were deemed sufficiently accurate to use and helped to expand and refine the MARVEL network. The vast majority of existing data covers the A-X band with variable accuracy, with some papers, particularly older ones, not providing uncertainties at all and, in the case of 80CoHeMo (Cosby et al. 1980), not assigning their transitions. This means that the observed frequencies cannot be added to the MARVEL network, where the nodes are characterized by the quantum numbers of the energy levels involved. There is only comprehensive MARVEL energy level data (extending up to high J) for vibrational states with $v = 0$–$3/4$ for both electronic states, and some limited data for $A\,^1\Pi$ $v = 11 - 14$.

MARVEL analyses uncertainty when evaluating transition data and is able to determine whether or not an uncertainty is consistent with the other data. Using this, the quoted experimental uncertainties for the older sources 42DoHe (Douglas & Herzberg 1942), 60DoMo (Douglas & Morton 1960), and 81GrBrOkWi (Grieman et al. 1981) were increased to allow MARVEL to become self-consistent. After this it was only necessary to exclude two lines from the network: the 06PeDr pure rotational line and the 60DoMo A-X $v = 2 - 1$ P(8) line.

The MARVEL input transitions file and output energies file are given as Supporting Information to this paper. Table 2 summarizes the available high-resolution spectroscopic data for $^{13}CH^+$; with less than half the number of lines available for $^{12}CH^+$; there are insufficient spectroscopic data to perform a useful MARVEL study for $^{13}CH^+$.

2.2 Calculations (LEVEL)

Version LEVEL-16 (Le Roy 2017) was used to compute the line list. This solves the radial Schrödinger equation to give vibrational and rotational energy levels within a defined potential, as well as transition frequencies and Einstein coefficients for the coupling within or between potentials. LEVEL was chosen as the existing work on CH^+ by Cho & Le Roy (2016) used features in this program that are not easy to reproduce with other nuclear motion programs.

The effective radial Schrödinger equation used in this study as given by Cho & Le Roy (2016) is

$$\left\{-\frac{\hbar^2}{2\mu}\frac{\mathrm{d}^2}{\mathrm{d}r^2} + V_i(r) + \frac{\left[J(J+1)-\Lambda^2\right]\hbar^2}{2\mu r^2}\left[1+g_i(r)\right]\right\}\psi_{v,J}(r) = E_{v,J}\,\psi_{v,J}(r), \quad (1)$$

where μ is the reduced mass and Λ represents the projection of electronic orbital angular momentum on the internuclear axis. $V_i(r)$ is the adiabatic PEC of electronic state i that can include Born–Oppenheimer breakdown (BOB) functions and $g_i(r)$ describes centrifugal BOB function; see Cho & Le Roy (2016) for more detail on these BOB functions. The levels in the $A\,^1\Pi$ state of CH^+ have $\Lambda = 1$ and its levels are split by Λ-doubling, the magnitude of which

Table 2. Summary of high-resolution spectroscopic laboratory studies of $^{13}CH^+$.

Reference	Freq. range (cm^{-1})	Detected transitions[a]	*A*
Antić-Jovanovic et al. (1983)	20800–26700	$A\,^1\Pi$ - $X\,^1\Sigma^+$ (0,0), (0,1), (1,0), (2,1), (2,0), (3,1); $J \leq 12$	151
Bembenek (1997)	20800–26700	$A\,^1\Pi$ - $X\,^1\Sigma^+$ (0,0), (0,1), (1,1), (1,0), (2,2), (2,1); $J \leq 9$	95
Amano (2010b)	27.	(0,0): R(0)	1
Yu et al. (2018)	27.8–82.3	(0,0): R(1), R(2), R(3)	3
Domenech et al. (2018)	27.8, 2711–2817	(0,0): R(1); (1,0): P(1), R(1), R(2), R(3)	5

Notes. [a]Bracketed values indicate the vibrational bands involved in transition, (v', v'').
[b]'A': number of actual lines in source.

depends on *J*, see Helm et al. (1982b); Cho & Le Roy included a *J*-dependent term in the potential to incorporate the effects of Λ-doubling, as follows

$$sg(e/f)\Delta V_\Lambda(r)\,[J(J+1)]^\Lambda = sg(e/f)\left\{\left(\frac{\hbar^2}{2\mu r^2}\right)^{2\Lambda} f_\Lambda(r)\right\}[J(J+1)]^\Lambda, \quad (2)$$

where $sg(e/f) = +1$ and 0 for *e* and *f* levels respectively (in accordance with the form suggested later by Yu et al. 2018), and $f_\Lambda(r)$ is a Λ-doubling radial strength function with the following form, also determined by Cho & Le Roy

$$f_\Lambda(r) = \sum_{i=0}^{4} \omega_i y_{p_\Lambda}^i \quad (3)$$

with

$$y_{p_\Lambda}(r) = \frac{r^{p_\Lambda} - r_e^{p_\Lambda}}{r^{p_\Lambda} + r_e^{p_\Lambda}}, \quad (4)$$

where ω_i are expansion coefficients, $r_e = 1.235896$ Å is the equilibrium internuclear distance for the $A\,^1\Pi$ state potential, and $p_\Lambda = 4$, all determined and given in Cho & Le Roy (2016). Solving equation (1) for each of the two electronic state potentials, $V_i(r)$, yields the vibrational and rotational eigenfunctions (energy levels) that form the basis of the line list.

2.2.1 *Potential energy and dipole moment curves*

The CH^+ input file created for use in LEVEL by Cho & Le Roy (2016) was used as a basis in this study. Our investigation was limited to the ground and first excited singlet states, $X\,^1\Sigma^+$ and $A\,^1\Pi$, as investigated by Cho & Le Roy. As shown in Fig. 1, these are the only singlet states below the first dissociation limit, and any spin-forbidden transitions between these states and the low-lying triplet ($a\,^3\Pi$) state are yet to be observed and likely to be extremely weak (Gao et al. 2017). Spin–orbit coupling to this state was also neglected. Fig. 1 does not resolve the C^+ ion fine structure at dissociation but we note that $X\,^1\Sigma^+$ actually correlates with the lower of the two fine structure levels (Bazet et al. 1975), while the $A\,^1\Pi$ state dissociates to the upper fine structure level.

The full, empirical PECs calculated by Cho & Le Roy (2016) utilize previous spectroscopic data to characterize the curves more accurately than previous *ab initio* studies. Literature DMs (X-X and A-A) and TDMs (A-X) were compared to determined the most suitable available DM curves, see Fig. 2. Since all curves agree well, we chose those of Biglari et al. (2014), due to their comprehensive characterization of the curves up to high internuclear distance, *r*. We note that Mbiba Touedebe et al. (2023) also recently characterized these quantities, but their work only became available after we started calculations and hence was not considered in the initial analysis.

To get correct results it transpired that the basic input file provided by Cho & Le Roy (2016) required modification. We utilized the most recent version of LEVEL (LEVEL-16), but there were significant issues with the both input file and the LEVEL code itself. First, the input file gave incorrect values for several parameters which had to be investigated and corrected. For example, Λ being set to 0 for the $A\,^1\Pi$ and most of the parameters describing the $^{12}CH^+$ $X\,^1\Sigma^+$ ground state were set to values that describe the $^{12}CD^+$ $A\,^1\Pi$ excited state! Even when amended, the input file still gave errors when running with LEVEL. Analysis of the FORTRAN source code showed that in places the code disagreed with the documentation and input file structure on the ordering of parameters that read the input potential energy function; we therefore modified the LEVEL code to resolve these errors. As Cho & Le Roy (2016) did not consider transition probabilities, we then modified the input file to read in the DM/TDM functions and to instruct LEVEL to compute Einstein A coefficients. The final version of the LEVEL input file is provided as Supporting Information. The source for the modified LEVEL can be found at github.org/exomol. With these adjustments, we reproduced Cho & Le Roy (2016) to the four decimal places (0.0001 cm^{-1}) given by the LEVEL output they supply for $^{12}CH^+$. Some differences were found for $^{13}CH^+$ due to different treatments of the BOB terms.

2.2.2 Λ*-doubling*

LEVEL does not consider Λ-doubling, the splitting of rotational energy levels in $\Lambda > 0$ electronic states due to their *e*/*f*-parity. Λ-doubling is an important effect to consider, as without it our calculated energy levels in the $A\,^1\Pi$ state would be degenerate which is incorrect. Yu et al. (2018) analysed Λ-doubling in the CH^+ $A\,^1\Pi$ state where the effect arises due to the interactions of the *e*/*f* rotational levels with $^1\Sigma^+/^1\Sigma^-$ states, respectively. They found that treatment of this effect in all previous spectroscopic studies was incorrect as it was generally assumed that the Λ-doubling energy of *e*/*f* levels would lead to a symmetric shift in their energy terms, as the magnitude of the interaction of *e* levels with Σ^+ and *f* levels with Σ^- states was assumed to be equal. In practice, Yu et al. (2018) argued that the energy splitting is asymmetric with the *f* levels negligibly perturbed since Σ^- states will lie at much higher energy (none have so far been detected). In accordance with the findings of Yu et al. (2018), the $A\,^1\Pi$ state energies computed by LEVEL correspond to the energy of the unperturbed *f*-parity level. It is therefore necessary to account for the perturbed *e*-parity levels. Cho & Le Roy (2016) model the splitting by the inclusion of an additional term in the potential energy function of their radial Schrödinger equation, as described in equation (2), which shows that the *e*-parity energy level perturbation increases with J^2, whereas the *f*-parity levels are unperturbed. Since the version of LEVEL we used does not account for this, an empirical approach to considering the effect was taken.

Table 3. Λ-doubling correction calculation parameters, showing the original expectation value of the Λ-doubling operator for each vibrational level, the observed/calculated correction ratio and the resulting scaled calculated correction. Asterisks indicate extrapolated ratios. *J*-dependence can then be incorporated by evaluating the entirety of equation (2) using the scaled values to give the final correction to each *f*-state energy to account for Λ-doubling.

v	Original $\langle\psi_v\lvert\Delta V_\Lambda\rvert\psi_v\rangle$ (cm^{-1})	Average obs./calc. Ratio	Scaled $\langle\psi_v\lvert\Delta V_\Lambda\rvert\psi_v\rangle$ (cm^{-1})
0	0.000297	127.051	0.037787
1	0.000594	58.449	0.034727
2	0.001017	30.897	0.031434
3	0.001429	19.902	0.028440
4	0.001736	15.464∗	0.026851
5	0.001906	13.690∗	0.026096
6	0.001946	12.978∗	0.025261
7	0.001877	12.693∗	0.023827
8	0.001713	12.579∗	0.021553
9	0.001463	12.533∗	0.018334
10	0.001134	12.515∗	0.014188
11	0.000752	12.507∗	0.009402
12	0.000384	12.504∗	0.004800
13	0.000136	12.503∗	0.001704
14	0.000026	12.503∗	0.000322

The approach taken consisted of separately calculating a correction to each *f*-parity rotational level within each vibrational level of the $A\,^1\Pi$ state, which could be applied to give the energy of the corresponding *e*-parity level. This involved computing the expectation value of the operator $\Delta V_\Lambda(r)$ given in equation (2) for each vibrational level, $\langle\psi_v\lvert\Delta V_\Lambda(r)\rvert\psi_v\rangle$, and evaluating the rotational *J*-dependence to give the energy level correction. To do this, the operator was calculated for each value of internuclear distance, *r*, in steps of 0.001 Å from $r_{\rm min}$ to $r_{\rm max}$ for each vibrational level, which ranged from 2100 gridpoints for $v = 0$ to 90 000 for $v = 14$. The value of the vibrational wavefunction, provided by LEVEL upon modification of the input file, was also gathered at each value of *r*. The expectation value, $\langle\psi_v\lvert\Delta V_\Lambda(r)\rvert\psi_v\rangle$, was then calculated by summing the contribution evaluated at each *r* value to give the overall expectation value for that vibrational level. This was repeated for all vibrational levels, and these values can be seen in column 2 of Table 3. Incorporating the *J* dependence by evaluating the entirety of equation (2) (multiplying these corrections by $J(J + 1)$) gave the correction for each rotational level within each vibrational level. These corrections were then simply added to the *f*-parity energy to obtain the perturbed *e*-parity energy.

To verify these calculations, comparison was made to observed (experimental) splittings, some of which were available from MARVEL data (where both *e* and *f* energies for the same rotational level were known). The calculations did not initially produce results in line with observational corrections, however, further investigation revealed that the ratio between the calculated and corresponding observed correction was generally constant within each vibrational level from $v = 0$ to 3, the region over which the MARVEL data was fairly comprehensive. Therefore, the calculated corrections within each vibrational level could be scaled by the average ratio to provide an accurate account of Λ-doubling in line with observation. The average ratio for each *v* can be seen in Fig. 3, showing an apparent exponentially decaying trend with increasing *v*. Unfortunately, due to the limited coverage of the MARVEL data, little information about higher *v* levels meant an extrapolation of the curve was necessary to estimate the ratio for higher *v* levels. The extrapolation was performed using an exponential fit and is shown in Fig. 3. From this,

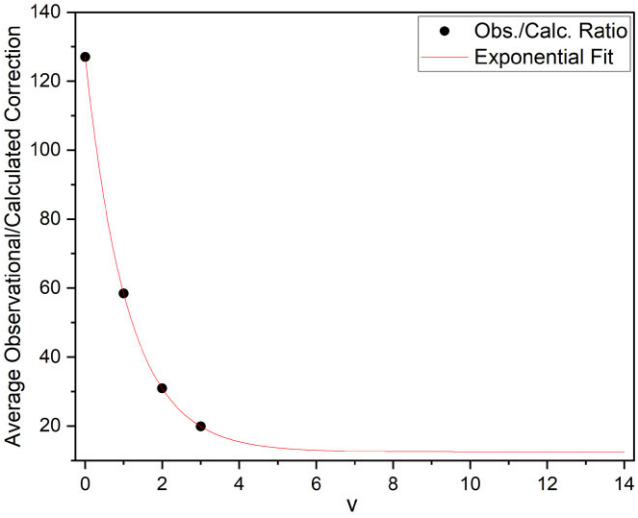

Figure 3. The average ratio of observed to calculated Λ-doubling correction ($e - f$ energy) plotted against vibrational level. An extrapolation to higher vibrational levels is performed using an exponential fit. Values of average ratio can be seen in Table 3 for all *v* levels.

the extrapolated ratio for $v \geq 4$ levels could be estimated, as seen by the asterisked values in column 3 of Table 3. With this, the calculated corrections for each level were scaled by the corresponding ratio to give the final correction for each *v* level, as can be seen in the final column of Table 3. After applying *J*-dependence, the final correction values for each level was added to the corresponding (*f*-state) energy to give that of the *e*-state. The scaling with observational corrections means this approach should be accurate for low *v*'s but the extrapolated corrections are less secure and would benefit from experimental confirmation.

We note that this treatment of Λ-doubling only considers the effect on the energies and therefore does not allow for possible intensity stealing effects with a perturbing $^1\Sigma^+$ state. Any such effect is likely to be small.

2.2.3 *Einstein coefficients*

LEVEL computes Einstein *A* coefficients using the expression

$$A_{v',\Lambda',J',v'',\Lambda'',J''} = 3.1361891 \times 10^{-7} \times \frac{S(J',\,\Lambda',\,J'',\,\Lambda'')}{2J'+1}\,\nu^3\,|\left\langle\Psi_{v',\Lambda',J'}|M(r)|\Psi_{v'',\Lambda'',J''}\right\rangle|^2, \quad (5)$$

where *A* is the Einstein coefficient (s^{-1}), $S(J',\,\Lambda',\,J'',\,\Lambda'')$ is the Hönl–London rotational intensity factor (Hansson & Watson 2005), J' the upper level rotational quantum number, ν the transition wavenumber (cm^{-1}), $\Psi_{v',\Lambda',J'}$ and $\Psi_{v'',\Lambda'',J''}$ the normalized initial and final states radial wavefunctions, and $\left\langle\Psi_{v',\Lambda',J'}|M(r)|\Psi_{v'',\Lambda'',J''}\right\rangle$ the expectation value of the DM/TDM function $M(r)$, which we asked LEVEL to output. We note that the use of a Hönl–London factor in equation (5) is not an approximation since the dipole matrix element used makes full allowance for the *J* and Λ dependence of the wavefunction. However, for the $A\,^1\Pi$ state wavefunctions other approximations come into play that are discussed below.

LEVEL's lack of consideration of Λ-doubling means *e*-parity $A\,^1\Pi$ levels are not present and transitions involving these states were not correctly accounted for. $A\,^1\Pi(e)$-X transitions were incorrectly assigned the wavenumber of the corresponding (forbidden by dipole selection rules) $A\,^1\Pi(f)$-X transition which led to an incorrect calcu-

lation of the Einstein A coefficient since equation (5) depends on the transition wavenumber. By applying the relevant $e - f$ correction to each transition wavenumber, the Einstein coefficient was recalculated using equation (5) and the outputted dipole matrix elements. For transitions within the $A\,^1\Pi$ state this required some care due to many transitions being unaccounted for, as potentially four transitions exist where LEVEL computes just one transition and thus one A coefficient that uses (often incorrect) transition information that LEVEL provided. For example, LEVEL gives Q-branch ($\Delta J = 0$) transitions within the same vibrational level a wavenumber of 0 cm^{-1}, but in reality these correspond to long wavelength, allowed Λ-doublet transitions between e and f states of the same rotational level. This meant calculating equation (5) in its entirety including determining the relevant Hönl–London factor (Hansson & Watson 2005). Note that these methods to recalculate the Einstein coefficient assume the expectation value of the DM/TDM function in equation (5) remains unchanged, which is in any case a common approximation used in other treatments and is unlikely to be problematic.

2.3 Final line lists

This above calculation procedure was followed for both $^{12}CH^+$ and $^{13}CH^+$ and line lists were generated considering states with J up to 68 and 69, respectively. For $^{12}CH^+$ one further step was performed. The MARVEL energy levels with associated uncertainties were used to replace the ones computed by LEVEL.

Due to the greater accuracy of the empirical MARVEL data, calculated $^{12}CH^+$ energies were replaced with the respective MARVEL values where available in the States file. These 'MARVELized' energy levels can be identified via the 'Label' column in the states file which indicates 'Ma' if the MARVEL energy level was used, or 'Ca' if there was no such available data. Note that the calculated energy prior to MARVELization is given in the 'Calc.' column. The uncertainty in the States file is determined depending on the energy level used. For the MARVELized energies, the uncertainty provided by MARVEL was simply used. For the calculated energies (which includes all $^{13}CH^+$ levels), an estimate for the uncertainty was made using the following expression:

$$\text{uncertainty} = av + bJ(J+1), \tag{6}$$

where $a = 0.05/0.1$ cm^{-1} and $b = 0.01/0.01$ cm^{-1} for are constant parameters for the $X\,^1\Sigma^+/A\,^1\Pi$ electronic states, respectively. These parameters were estimated by analysing the evolution of $^{12}CH^+$ obs. − calc. energy level residuals seen in Fig. 4, which plots the agreement of the MARVEL (obs.) and LEVEL (calc.) data and how this varies with v and J within each electronic state. Overall, the residuals were very small for low v and/or J levels of both the electronic states. Naturally, $A\,^1\Pi$ has greater residuals, especially for high v, since higher energies are probed and as a result of the manual treatment of Λ-doubling, but in general both states exhibit good accuracy. An apparent quadratic J dependence can be seen in the residuals in Fig. 4, motivating the form of equation (6).

3 RESULTS

3.1 Line list and file structure

With calculated energies for rotational and vibrational levels of $X\,^1\Sigma^+$ and $A\,^1\Pi$, and transition frequencies and Einstein coefficients for allowed transitions, the components of the line list of CH^+ were complete. In accordance with ExoMol format, this was reformatted

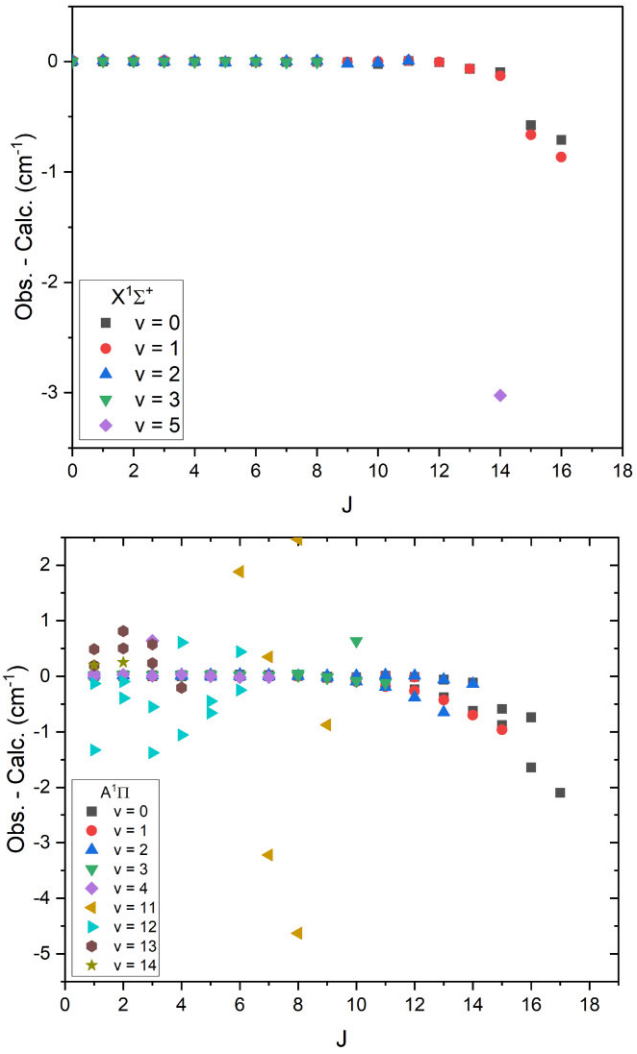

Figure 4. Obs. – Calc. residuals for the $X\,^1\Sigma^+$ (top) and $A\,^1\Pi$ (bottom) states for different vibrational levels as a function of J. Note that the two values for each (v, J) level in the $A\,^1\Pi$ plot are the e and f parity states, split by Λ-doubling.

into a States and Transitions file (Tennyson, Hill & Yurchenko 2013), extracts from which for $^{12}CH^+$ can be seen in Tables 4 and 5, respectively. The $^{12}CH^+$ States file contains 1505 rovibrational energy levels covering the $X\,^1\Sigma^+$ and $A\,^1\Pi$ electronic states up to a few thousand wavenumbers above the dissociation limit, additionally providing their uncertainty and associated quantum numbers defining the level. The Transitions file, characterizing 34 194 transitions, contains Einstein A coefficients and frequencies for each allowed transition between the energy levels of the States file. For $^{13}CH^+$, there are 1519 states and 42 387 transitions. We call these line lists PYT after the initial letter of the authors names.

It should be noted that, in the $^{12}CH^+$ Transitions file, all A-A transitions involving vibrational levels with $v \geq 4$ levels are excluded. This is due to further issues with LEVEL, which gave an error for these transitions. No A-A transitions have ever been detected and they are unlikely to be seen astronomically in the foreseeable future so this is not a significant defect.

Table 4. Extract from the States file for $^{12}CH^+$.

i	Energy (cm^{-1})	g_i	J	Unc. (cm^{-1})	τ (s)	+/−	e/f	State	v	Λ	Σ	Ω	Label	Calc.
367	24005.218550	134	33	11.470000	1.1470E + 01	−	e	$X\,^1\Sigma^+$	5	0	0	0	Ca	24005.218550
368	24038.829766	10	2	0.610000	6.1000E−01	+	e	$X\,^1\Sigma^+$	11	0	0	0	Ca	24038.829766
369	24072.559047	26	6	0.334901	3.3490E−01	−	f	$A\,^1\Pi$	0	1	0	1	Ma	24072.560989
370	24074.180657	26	6	0.217601	2.1760E−01	+	e	$A\,^1\Pi$	0	1	0	1	Ma	24074.148026
371	24091.232882	14	3	0.670000	6.7000E−01	−	e	$X\,^1\Sigma^+$	11	0	0	0	Ca	24091.232882
372	24107.338107	78	19	4.250000	4.2500E+00	−	e	$X\,^1\Sigma^+$	9	0	0	0	Ca	24107.338107
373	24131.807092	110	27	7.910000	7.9100E+00	−	e	$X\,^1\Sigma^+$	7	0	0	0	Ca	24131.807092
374	24160.970652	18	4	0.750000	7.5000E−01	+	e	$X\,^1\Sigma^+$	11	0	0	0	Ca	24160.970652
375	24162.245191	146	36	13.520000	1.3520E+01	+	e	$X\,^1\Sigma^+$	4	0	0	0	Ca	24162.245191
376	24165.617170	166	41	17.320000	1.7320E+01	−	e	$X\,^1\Sigma^+$	2	0	0	0	Ca	24165.617170
377	24229.503713	58	14	2.600000	2.6000E+00	+	e	$X\,^1\Sigma^+$	10	0	0	0	Ca	24229.503713
378	24229.561434	30	7	0.366501	3.6650E−01	+	f	$A\,^1\Pi$	0	1	0	1	Ma	24229.563130
379	24231.703209	30	7	0.204901	2.0490E−01	−	e	$A\,^1\Pi$	0	1	0	1	Ma	24231.679179
380	24247.929131	22	5	0.850000	8.5000E−01	−	e	$X\,^1\Sigma^+$	11	0	0	0	Ca	24247.929131
381	24351.966003	26	6	0.970000	9.7000E−01	+	e	$X\,^1\Sigma^+$	11	0	0	0	Ca	24351.966003
382	24408.044035	34	8	0.354901	3.5490E−01	−	f	$A\,^1\Pi$	0	1	0	1	Ma	24408.042265

Notes. i: state counting number, g_i: total statistical weight, J: total angular momentum, Unc: uncertainty (cm^{-1}), τ: lifetime (s), +/ −: total parity, *e/f*: rotational parity, v: vibrational level quantum number, Λ: projection of electronic angular momentum, Σ: projection of electron spin, Ω: projection of total angular momentum ($\Omega = \Lambda + \Sigma$), Label: 'Ma' denotes MARVEL energy level, 'Ca' denotes LEVEL calculated energy level, and Calc.: LEVEL calculated energy level value.

Table 5. Extract from the Transitions file for $^{12}CH^+$.

f	i	A_{fi} (s^{-1})	$\tilde{\nu}_{fi}$ (cm^{-1})
516	377	3.1861E+01	2754.475947
1178	759	1.1669E−09	2755.165546
92	58	1.5055E+00	2756.287971
658	473	3.9484E+00	2756.308088
544	392	2.8961E+01	2756.981308
266	210	2.5046E+01	2757.306730
1169	754	5.0213E−09	2757.533295
1161	748	1.9419E−02	2757.544843
991	674	2.2755E−03	2757.621535
612	440	1.0042E+01	2758.338556
1166	751	1.6578E−09	2758.406401
186	141	1.7163E+01	2758.513693
1298	774	1.1399E+01	2758.878845

Notes. f: final state counting number, i: initial state counting number, A_{fi}: Einstein A coefficient (s^{-1}), and $\tilde{\nu}_{fi}$: transition wavenumber (cm^{-1}).

3.2 Partition functions

A partition function for $^{12}CH^+$ was provided by Barklem & Collet (2016) for 42 temperatures up to 10 000 K. The program ExoCross (Yurchenko, Al-Refaie & Tennyson 2018) was used to calculate the partition function for both $^{12}CH^+$ and $^{13}CH^+$ in steps of 1 up to 10 000 K. The ExoMol convention, in accordance with HITRAN (Gamache et al. 2017), is to provide partition functions that include full atomic nuclear spin degeneracy, g_{ns}. For $^{12}C^1H^+$, this gives a value of 2, while for $^{13}CH^+$ it gives 4. As such, the values of the $^{12}CH^+$ partition function of Barklem and Collet, who do not account for this, have been multiplied by 2 for comparison, which can be seen in Fig. 5. Very good agreement can be seen below about 3000 K. At higher temperatures, agreement decreases somewhat which is likely due to the increasingly significant thermal occupation of higher energy electronic states that were not considered in this study, most notably the $a\,^3\Pi$ state which lies between $X\,^1\Sigma^+$ and $A\,^1\Pi$. As a result, a maximum temperature of 5000 K has been shown. JPL also provided a $^{12}CH^+$ partition function for several low temperatures, the largest of which, at 300 K, 30.7006 (Pickett et al. 1998, again after accounting for nuclear spin degeneracy) shows excellent agreement with the calculated value here of 30.6990.

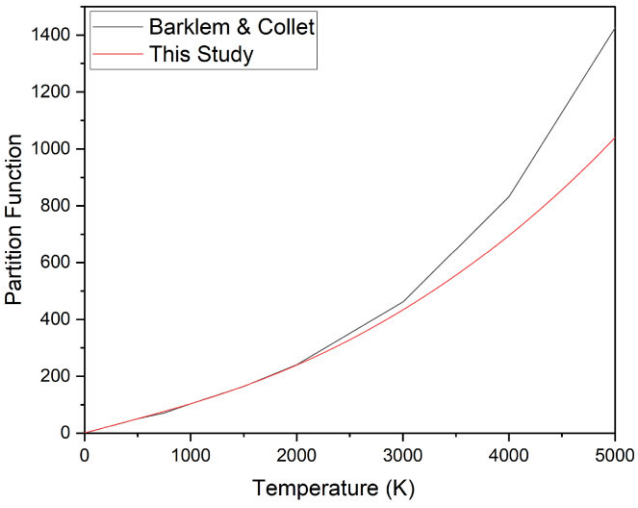

Figure 5. CH^+ partition function as calculated from the line list by ExoCross compared with that of Barklem & Collet (2016).

3.3 Spectra

Using the PYT $^{12}CH^+$ line list, ExoCross (Yurchenko et al. 2018) was used to simulate absorption/emission spectra at various temperatures. Fig. 6 shows simulated absorption spectra for temperatures of 296 and 2000 K. A Doppler broadened Gaussian profile that is dependent on temperature has been used. The spectra have been separated with rotational and vibrational spectra in the top panel and electronic in the bottom, to avoid large gaps in the plot. Note that a logarithmic intensity scale has been used to show the relatively weak vibrational (IR) spectrum (seen for the wavenumber >1000 cm^{-1} region of the top-panel plots) compared to the rotational and electronic spectrum.

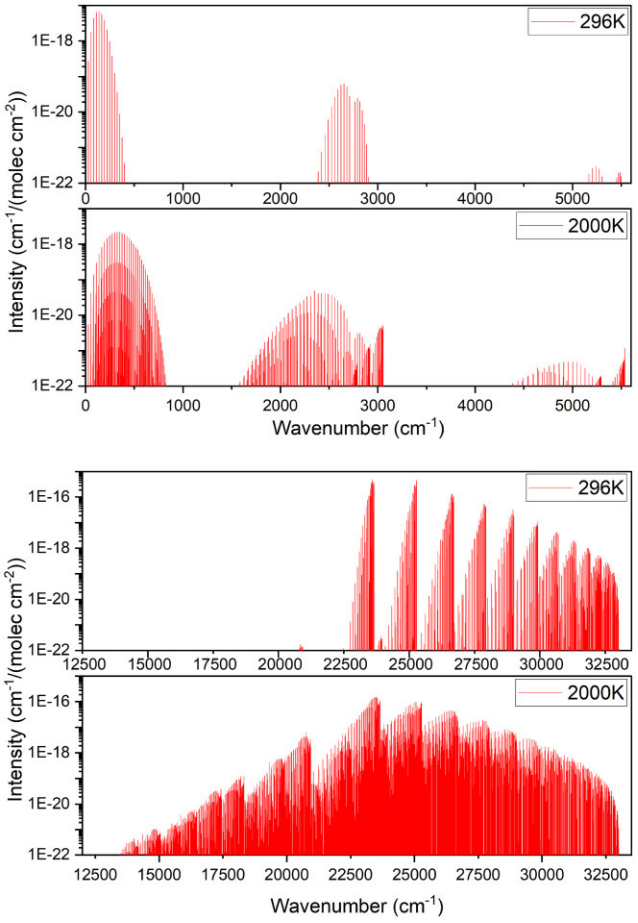

Figure 6. Simulated absorption spectra at 296 and 2000 K, covering the rotational and vibrational (IR) bands (top) and the electronic bands (bottom). Spectra produced using a Doppler broadened profile with ExoCross.

This corroborates the elusiveness of this spectrum as noted by previous studies.

To assess the quality of the calculated line list, comparison with previously recorded spectra are made. As no prior line list for CH^+ exists, nor an experimental/observational spectrum covering an extensive wavelength range, comparison are made to selected portions of the full spectrum.

Low-lying pure rotational transitions of CH^+ have been previously measured, as seen in Table 1, but no rotational spectra are presented. However, the JPL spectroscopy database (Pickett et al. 1998), who also aim to provide spectroscopic data for molecular transitions, used the first laboratory detection of the $J = 1 - 0$ CH^+ rotational line (Pearson & Drouin 2006) along with previous electronic A-X band data to generate a predicted rotational spectrum up to $J = 8$. Although, as discussed previously, this laboratory detection was later found to be inaccurate by 0.0019 cm^{-1}, and a wider range of rotational lines have since been detected both in the lab and in space, JPL has not updated their database and the inaccurate data is still presented. Nevertheless, this discrepancy would not be visible on the scale of comparing multiple lines and their intensities should still be accurate, as such the JPL rotational spectrum of CH^+ has been compared with the calculations of this study in Fig. 7. The simulated stick spectrum from ExoCross was run at a temperature of 300 K to match that of JPL, and the JPL intensities were converted to standard ExoMol/HITRAN units of cm molecule^{-1} for comparison. In Fig. 7,

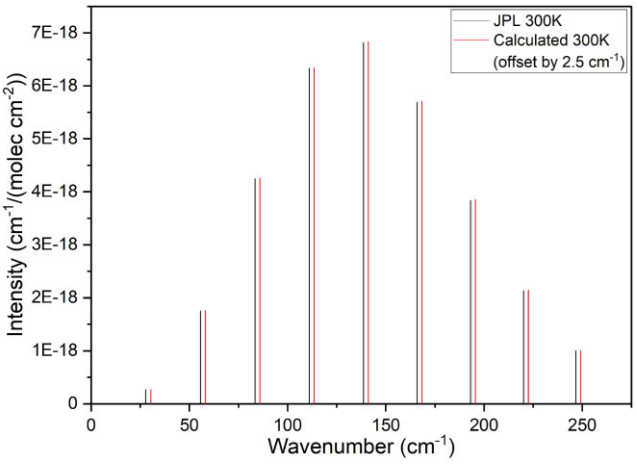

Figure 7. Comparison of the JPL CH^+ $X\,^1\Sigma^+$ rotational spectrum (black) with the calculated rotational stick spectrum from this study (red). Note that the calculated data have been offset by 2.5 cm^{-1} for intensity comparison.

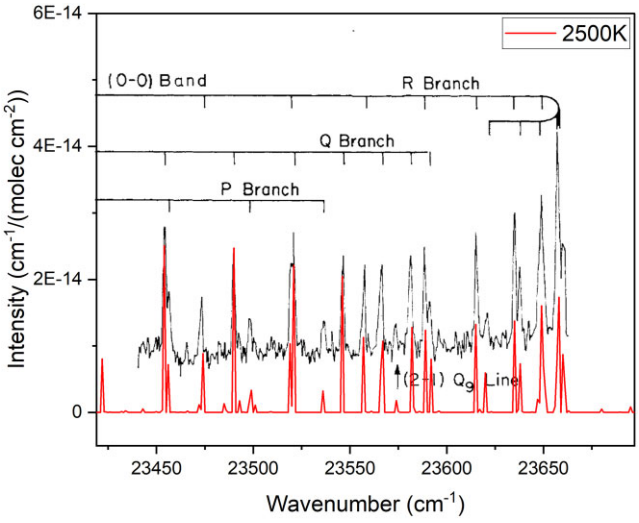

Figure 8. Comparison of the $v = 0 - 0$ $A\,^1\Pi - X\,^1\Sigma^+$ band spectrum from Grieman et al. (1981) (upper) with the simulated emission spectrum from ExoCross at 2500 K (lower). A Doppler line profile was used. The intensity scale corresponds only to the calculated ExoCross data, since Grieman et al. provided arbitrary units.

the calculated spectrum of this study has been offset by $+2.5$ cm^{-1} to allow for visual comparison, as the wavenumbers agree to a high degree of accuracy. The intensities can also be seen to agree closely.

The weak nature of the vibrational (IR) spectrum of CH^+ means it has only been detected in one astrophysical object (Neufeld et al. 2021) and one laboratory study (Domenech et al. 2018), of which no presented spectra exist, so visual comparison cannot be made. The A-X electronic spectrum is by far the most studied of CH^+ with many experimental studies focusing on the molecule, however, presented spectra are limited. A study by Grieman et al. (1981) used laser-induced fluorescence to probe CH^+ emission and presented a portion of the $v = 0 - 0$ band of the A-X spectrum, a comparison to which, using a simulated emission spectrum, has been shown in Fig. 8. The previous study also gave arbitrary intensity units and is probably not recorded in sample in thermodynamic equilibrium, so the intensity pattern is not expected to match that of this study. As

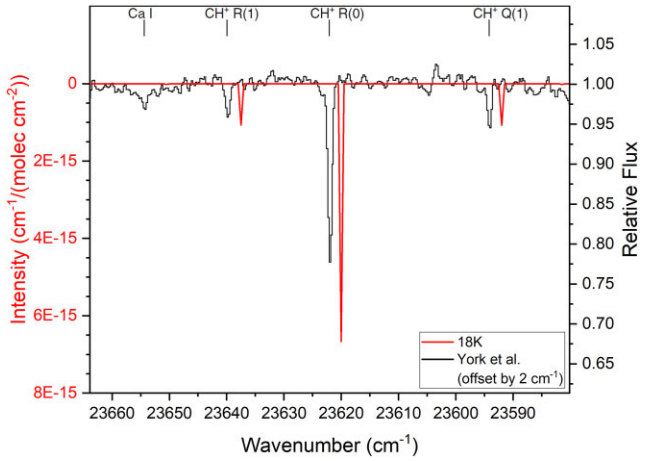

Figure 9. Comparison of the A-X spectral lines of the DIBs observed towards *Herschel* 36 York et al. 2013) with the simulated absorption spectrum of this study at 18 K (slightly blue shifted), for which a Doppler line profile is used. The units on the left axis correspond to the calculated data of this study, while the units on the right correspond to the intensity units provided by the DIB study. Note that wavenumber increases right to left as the original DIB study used wavelength units. The DIB data were originally blueshifted by $\sim$+6.75 cm^{-1} ($-$1.21 Å), after aligning the two spectra, the DIB data were offset by $+2$ cm^{-1} (to the left) for clearer intensity comparison.

such, a temperature of 2500 K was somewhat arbitrarily chosen for our calculated spectrum based on the high temperature requirement and certain similarities in intensity pattern. On Fig. 8, the intensity units correspond only to the results of this study (red). The spectrum from the previous study had to be offset slightly to match the spectrum of this study which indicates a slight error in their axes, since the transition wavenumbers of the two studies match to a high degree of accuracy.

CH^+ A-X absorption was seen in diffuse interstellar bands (DIBs) along the line of sight towards star system *Herschel* 36 and three lines were detected (York et al. 2013), R(0), R(1), and Q(1). A comparison to the spectra of these is shown in Fig. 9. Note that since the study used wavelength units for their spectrum, wavenumber increases right to left. Upon analysis, the DIBs were observed to be blueshifted relative to the calculated lines with an offset of approximately $+6.75$ cm^{-1} ($-$1.21 Å, indicating the absorbing object is moving at 85.7 km s^{-1} towards us). After matching the line positions, an offset of $+2$ cm^{-1} (to the left) was applied to the DIB data to allow for visual comparison of the intensities. The red intensity units correspond to calculated data, while the black relative flux units correspond to the DIB study. Since the temperature of the absorption region was not found in the previous study, spectra were simulated at various temperatures using ExoCross to match up the intensity pattern of the observed lines, which would be expected to agree between these two studies. It appears that a temperature of 18 K matches the $J = 1$ lines well (by eye) while overestimating the observed $J = 0$ line flux. A temperature higher than 18 K results in an intensity decrease from $J = 0$ levels but an increase from $J = 1$ levels (it is assumed that thermal population of a rotational level is proportional to the intensity of transitions from that level). Thus, the intensity of the $J = 0$ and 1 lines on the above spectra cannot both match up. This suggests that the region is consistent with a temperature of 18 K, but that the observed $J = 0$ line is optically thick, and thus is limited in its intensity.

3.4 Einstein coefficients, lifetimes, and oscillator strengths

A number of early experimental (Brooks & Smith 1975; Erman 1977; Becker, Brenig & Tatarczyk 1980; Mahan & O'Keefe 1981) and theoretical (Yoshimine, Green & Thaddeus 1973; Dalgarno 1976; Larsson & Siegbahn 1983) studies considered the lifetimes of excited states of CH^+ and/or the associated oscillator strengths. The most recent and probably most reliable of the experimental studies by Mahan & O'Keefe (1981) gave a lifetime for the $v = 0$ state of A $^1\Pi$ of 815 $\pm$ 25 ns, some 30 per cent larger than previous measurements but in good agreement (i.e. within 15 per cent) of the prevailing theoretical studies. Our calculated value for both $J = 1$, $v = 0$ A $^1\Pi$ states is 910 ns, about 10 per cent higher than this value. The lifetime, τ_i, for state i was computed using the following relation (Tennyson et al. 2016)

$$\tau_i = \frac{1}{\sum_f A_{fi}}, \tag{7}$$

where A_{fi} are the appropriate Einstein A coefficients. All lifetimes are given as part of the States file, see Table 4. Note that our treatment of lifetimes does not consider the effects of predissociation or possible interactions with other electronic states; these effects are only significant in the region above the dissociation limit.

Most theoretical studies have concentrated on oscillator strengths rather than lifetimes, although of course the two are related. We note that the theoretical studies cited above all used the Franck–Condon approximation, which is known not to work particularly well for CH^+ (Yoshimine et al. 1973), and neglected any dependence on rotation; these approximations neglect a number of effects including the r dependence of the TDM. Our calculations make neither of these approximations. In the Supporting Information, we provide a list of our oscillator strengths connecting the X $^1\Sigma^+$ $v'' = 0$, $J'' = 0$ state and A $^1\Pi$ v', $J' = 1$ states for both $^{12}CH^+$ and $^{13}CH^+$, although values for the two isotopologues are essentially the same. Weselak et al. (2009) consider the ratio of oscillator strengths for transitions between the X $^1\Sigma^+$ $v'' = 0$ state and A $^1\Pi$ v' states as a ratio to the $v'' = 0 - v' = 0$ transition (values of J are not considered). Our oscillator strength value for $(v', v'') = (0, 0)$ is 0.00501, slightly lower than the calculated value of 0.00545 due to Larsson & Siegbahn (1983) recommended by Weselak et al. (2009), in line with our slightly longer predicted lifetimes compared to previous studies. Our ratios between oscillator strengths are in reasonable agreement with previous calculated ratios, within 6 per cent, except for the much weaker (4,0) overtone band, where it is 13 per cent. It is not uncommon for the intensity of weaker, high overtone bands to be predicted with lower accuracy. We note, however, that Weselak et al. (2009) used the Franck–Condon approximation as part of their statistical analysis of high-resolution echelle stellar spectra, which is also known to degrade with vibrational excitation.

Einstein A coefficients for transitions with the X $^1\Sigma^+$ state can be compared with the work of Changala et al. (2021) who analysed unusual CH^+ rovibrational emission patterns in NGC 7027 and gave Einstein coefficients for R- and P-branch transitions in the $v = 1 - 0$ band in an attempt to explain unexpectedly weak R-branch transitions. The calculated coefficients of this study have been compared with these in Table 6. The Einstein coefficients are seen to agree well, which supports the observation of weaker R-branch transitions. Changala et al. (2021) also used PECs from Cho & Le Roy (2016), so the differences in results likely lies with differences in fitting, or the differing DMs used. Despite this, since the DMs for these vibrational transitions are so small (hence the weakness of the

Table 6. Comparison of Einstein A coefficients for the $v = 1 - 0$ band of $X\,^1\Sigma^+$ from Changala et al. (2021) to those of this study. Rotation transitions are denoted using the standard P(J") and R(J") notation.

Transition	Changala et al.	This study	Transition	Changala et al.	This study	Transition	Changala et al.	This study
R(19)	2.88283	3.03821	**R(5)**	0.09044	0.06712	**P(9)**	4.09076	3.93378
R(18)	2.41605	2.55795	**R(4)**	0.18326	0.14975	**P(10)**	4.37871	4.21857
R(17)	1.98722	2.11561	**R(3)**	0.30131	0.25858	**P(11)**	4.65704	4.49416
R(16)	1.59804	1.71294	**R(2)**	0.43506	0.38462	**P(12)**	4.9231	4.75791
R(15)	1.24991	1.35135	**R(1)**	0.56372	0.50836	**P(13)**	5.17457	5.00751
R(14)	0.94394	1.03198	**R(0)**	0.61818	0.56547	**P(14)**	5.40944	5.24094
R(13)	0.68091	0.75564	**P(1)**	2.87367	2.67911	**P(15)**	5.62596	5.45643
R(12)	0.46122	0.52277	**P(2)**	2.28988	2.14908	**P(16)**	5.82263	5.65251
R(11)	0.28493	0.33346	**P(3)**	2.41302	2.27697	**P(17)**	5.99824	5.82790
R(10)	0.15172	0.18743	**P(4)**	2.64446	2.50664	**P(18)**	6.15178	5.98161
R(9)	0.06085	0.08400	**P(5)**	2.91483	2.77344	**P(19)**	6.2825	6.11286
R(8)	0.01117	0.02207	**P(6)**	3.20295	3.05749	**P(20)**	6.38985	6.22109
R(7)	0.00108	0.00009	**P(7)**	3.49882	3.34926			
R(6)	0.02845	0.01601	**P(8)**	3.79625	3.64282			

observed transitions), the level of disagreement between results is unproblematic.

4 DISCUSSION AND CONCLUSIONS

A rovibronic line list has been calculated for the $X\,^1\Sigma^+$ and $A\,^1\Pi$ states of $^{12}CH^+$ and $^{13}CH^+$ for the first time; the PYT line lists provide energy levels with uncertainties, transition frequencies, and Einstein A coefficients. The states, transition, and partition function files for the PYT line lists can be downloaded from www.exomol.com or zenodo.

The line list is used to generate absorption and emission spectra, as well as partition functions, which help to visualize the line list and provide a comparison to previous studies. The $^{12}CH^+$ line list is naturally very accurate for $v = 0 - 3$ of both states where empirical energy levels are comprehensive. The calculated levels, making up the line list outside the realm of observational data, are more uncertain but our analysis shows that the calculations reproduce experimental line frequencies well (to $\lesssim 0.01$ cm^{-1}) up to at least $J = 12$ for $X\,^1\Sigma^+$ and $A\,^1\Pi(f)$ states. Residuals in $A\,^1\Pi(e)$ states are expectedly larger than their f counterparts since their energies were calculated with an approximate treatment of Λ-doubling. These show still accuracies to at least $\sim$0.01 cm^{-1} for $J \leq 9$; however, the lack of observational data for $v \geq 4$ means these data should be treated with more caution. In general, agreement is better in the lower energy $X\,^1\Sigma^+$, as expected, and in both states residuals increase with greater v and exhibit an apparent J^2 dependence at high J. Such levels are high in energy (e.g. the lowest $A\,^1\Pi$ level is over 23 600 cm^{-1} above that of $X\,^1\Sigma^+$) meaning that the discrepancy is likely due, in part, to interaction with more highly excited electronic states that has not been considered here, such as spin–orbit coupling, which becomes increasingly important at higher energies and may perturb energy levels. Note that, where residuals are relatively large, the MARVEL (obs.) data are also more uncertain, since these high-energy levels are typically determined by just one observed transition (usually multiple are available) yielding uncertainties of the order 1–3 cm^{-1} for the few $v \geq 4$ empirical levels in both $X\,^1\Sigma^+$ and $A\,^1\Pi$ states.

The PYT line lists for $^{12}C^1H^+$ and $^{13}C^1H^+$ comprehensively characterizes well above and beyond the domain of previous observation. Identification of future avenues of research, dependent on later observation, have also been presented. The accuracy and completeness of the line list open up its potential application to future high-resolution studies and any hot observations of CH^+, as well as the investigation of a range of astronomical environments, including the complex chemistry of interstellar clouds.

ACKNOWLEDGEMENTS

This work was supported by the European Research Council (ERC) under the European Union's Horizon 2020 research and innovation programme through advance grant no. 883830 and the Science an Technology Funding Council (STFC) projects nos ST/M001334/1 and ST/R000476/1. We thank Nike Dattani for providing the copy of LEVEL which we adapted for this study.

DATA AVAILABILITY

The states, transition, and partition function files for the $^{12}CH^+$ and $^{13}CH^+$ line lists can be downloaded from www.exomol.com and zenodo. Inputs for LEVEL, the $^{12}CH^+$ MARVEL energies and transitions files, a list of $(v', J' = 1) - (v'' = 0, J'' = 0)$ oscillator strengths and a readme file are provided as Supporting Information to this article. ExoCross and our adapted version of LEVEL are available at github.org/exomol.

REFERENCES

Amano T., 2010a, J. Chem. Phys., 133, 244305
Amano T., 2010b, ApJ, 716, L1
Amano T., 2015, in Simos T. E., Maroulis G., eds, AIP Conf. Proc. Vol. 1642, Proceedings of the International Conference of Computational Methods in Sciences and Engineering 2010 (ICCMSE-2010). p. 317
Amano T., Pearson J., Drouin B., Yu S., 2015, in Simos T E, Maroulis G, eds, Proceedings of the International Conference of Computational Methods in Sciences and Engineering 2010 (ICCMSE-2010). 1642, 317, American Institute of Physics, College Park, Maryland, USA
Antić-Jovanovic A., Bojović V., Pešić D. S., Weniger S., 1983, Spectrosc. Lett., 16, 11
Babb J. F., McLaughlin B. M., 2017, MNRAS, 468, 2052
Barinovs G., van Hemert M. C., 2004, Chem. Phys. Lett., 399, 406
Barklem P. S., Collet R., 2016, A&A, 588, A96
Bazet J. F., Harel C., McCarroll R., Riera A., 1975, A&A, 43, 229
Becker K. H., Brenig H. H., Tatarczyk T., 1980, Chem. Phys. Lett., 71, 242
Bembenek Z., 1997, J. Mol. Spectrosc., 181, 136
Bembenek Z., Cisak H., Kepa R., 1987, J. Phys. B: At. Mol. Opt. Phys., 20, 6197
Biglari Z., Shayesteh A., Maghari A., 2014, Comput. Theor. Chem., 1047, 22
Botterud I., Lofthus A., Veseth L., 1973, Phys. Scr., 8, 218

Brooks N. H., Smith W. H., 1975, ApJ, 196, 307
Carrington A., Ramsay D. A., 1982, Phys. Scr., 25, 272
Carrington A., Softley T. P., 1986, Chem. Phys., 106, 315
Cernicharo J., Liu X. W., Gonzalez Alfonso E., Cox P., Barlow M. J., Lim T., Swinyard B. M., 1997, ApJ, 483, L65
Chakrabarti K., Dora A., Ghosh R., Choudhury B. S., Tennyson J., 2017, J. Phys. B: At. Mol. Opt. Phys., 50, 175202
Changala P. B., Neufeld D. A., Godard B., 2021, ApJ, 917, 16
Cho Y.-S., Le Roy R. J., 2016, J. Chem. Phys., 144, 024311
Cosby P. C., Helm H., Moseley J. T., 1980, ApJ, 235, 52
Crane P., Lambert D. L., Sheffer Y., 1995, ApJS, 99, 107
Crawford I. A., 1989, MNRAS, 241, 575
Dalgarno A., 1976, in Burke P. G., Moiseiwitsch B. L., eds, Atomic Processes and Application. Elsevier, p. 109
Domenech J. L., Jusko P., Schlemmer S., Asvany O., 2018, ApJ, 857, 61
Douglas A., Herzberg G., 1942, Can. J. Phys., 20, 71
Douglas A. E., Morton J. R., 1960, ApJ, 131, 1
Dubois I., Lefebvre P. H., 2004, Mol. Phys., 102, 23
Dunham T., 1937, PASP, 49, 26
Erman P., 1977, ApJ, 213, L89
Falgarone E. et al., 2010, A&A, 521, L15
Falgarone E. et al., 2017, Nature, 548, 430
Faure A. et al., 2017, MNRAS, 469, 612
Furtenbacher T., Császár A. G., Tennyson J., 2007, J. Mol. Spectrosc., 245, 115
Gamache R. R. et al., 2017, J. Quant. Spectrosc. Radiat. Transfer, 203, 70
Gao Y., Wu T., Wan M., 2017, Comput. Theor. Chem., 1117, 276
Godard B., Pineau des Forêts G., Hennebelle P., Bellomi E., Valdivia V., 2023, A&A, 669, A74
Gredel R., 1997, A&A, 320, 929
Gredel R., Van Dishoeck E. F., Black J. H., 1993, A&A, 269, 477
Grieman F. J., Mahan B. H., O'Keefe A., Winn J. S., 1981, Faraday Discuss., 71, 191
Hakalla R., Kępa R., Szajna W., Zachwieja M., 2006, Eur. Phys. J. D, 38, 481
Hakalla R., Kepa R., Szajna W., Zachwieja M., 2007, Acta Phys. Pol. A, 111, 821
Hansson A., Watson J. K. G., 2005, J. Mol. Spectrosc., 233, 169
Hechtfischer U., Williams C., Lange M., Linkemann J., Schwalm D., Wester R., Wolf A., Zajfman D., 2002, J. Chem. Phys., 117, 8754
Hechtfischer U., Rostas J., Lange M., Linkemann J., Schwalm D., Wester R., Wolf A., Zajfman D., 2007, J. Chem. Phys., 127, 204304
Helm H., Cosby P. C., Graff M. M., Moseley J. T., 1982a, Phys. Rev. A, 25, 304
Helm H., Cosby P. C., Saxon R. P., Huestis D. L., 1982b, J. Chem. Phys., 76, 2516
Hobbs L. M., Thorburn J. A., Oka T., Barentine J., Snow T. P., York D. G., 2004, ApJ, 615, 947
Kanzler A. W., Sun H. S., Freed K. F., 1991, Int. J. Quantum Chem., 39, 269
Kowalski K., Piecuch P., 2001, Chem. Phys. Lett., 347, 237
Krelowski J., Galazutdinov G. A., Bondar A., 2020, Astron. Nachr., 341, 56
Larsson M., Siegbahn P. E. M., 1983, Chem. Phys., 76, 175
Le Roy R. J., 2017, J. Quant. Spectrosc. Radiat. Transfer, 186, 167
Mahan B. H., O'Keefe A., 1981, ApJ, 248, 1209
Mbiba Touedebe C., Nkem C., Owono Owono L. C., 2023, Mol. Phys., 121, e2151946
Mueller H. S. P., 2010, A&A, 514, L6
Muller S. et al., 2017, A&A, 606, A109
Naylor D. A. et al., 2010, A&A, 518, L117
Neufeld D. A., Godard B., Changala P. B., Faure A., Geballe T. R., Guesten R., Menten K. M., Wiesemeyer H., 2021, ApJ, 917, 15
Pearson J. C., Drouin B. J., 2006, ApJ, 647, L83
Pickett H. M., Poynter R. L., Cohen E. A., Delitsky M. L., Pearson J. C., Müller H. S. P., 1998, J. Quant. Spectrosc. Radiat. Transfer, 60, 883
Rangwala N. et al., 2011, ApJ, 743, 94
Ritchey A. M., Welty D. E., Dahlstrom J. A., York D. G., 2015, ApJ, 799, 197
Sarre P. J., Walmsley J. M., Whitham C. J., 1986, J. Chem. Soc. Faraday Trans. II, 82, 1243
Sarre P. J., Whitham C. J., Graff M. M., 1989, J. Chem. Phys., 90, 6061
Sauer S. P. A., Spirko V., 2013, J. Chem. Phys., 138, 024315
Saxon R. P., Kirby K., Liu B., 1980, J. Chem. Phys., 73, 1873
Stahl O., Casassus S., Wilson T., 2008, A&A, 477, 865
Tennyson J., Yurchenko S. N., 2012, MNRAS, 425, 21
Tennyson J., Hill C., Yurchenko S. N., 2013, in AIP Conf. Proc. Vol. 1545, 8th International Conference on Atomic and Molecular Data and their Applications ICAMDATA-2012. AIP, New York, p. 186
Tennyson J., Hulme K., Naim O. K., Yurchenko S. N., 2016, J. Phys. B: At. Mol. Opt. Phys., 49, 044002
Thi W. F. et al., 2011, A&A, 530, L2
Valdivia V., Godard B., Hennebelle P., Gerin M., Lesaffre P., Le Bourlot J., 2017, A&A, 600, A114
Vidal-García A. et al., 2022, EPJ Web Conf., 265, 00045
Weselak T., Galazutdinov G. A., Musaev F. A., Beletsky Y., Krełowski J., 2009, A&A, 495, 189
Wesson R. et al., 2010, A&A, 518, L144
York D. G. et al., 2013, in Proc. IAU Symp. 9: The Diffuse Interstellar Bands. J. Cami & N. L. J. Cox, Cambridge University Press, Cambridge, UK, p. 89
Yoshimine M., Green S., Thaddeus P., 1973, ApJ, 183, 899
Yu S., Drouin B. J., Pearson J. C., Amano T., 2018, J. Mol. Spectrosc., 350, 30
Yurchenko S. N., Al-Refaie A. F., Tennyson J., 2018, A&A, 614, A131

SUPPORTING INFORMATION

Supplementary data are available at *MNRAS* online.

suppl_data

Please note: Oxford University Press is not responsible for the content or functionality of any supporting materials supplied by the authors. Any queries (other than missing material) should be directed to the corresponding author for the article.

This paper has been typeset from a TEX/LATEX file prepared by the author.